Journal of Physics:
Conference Series

PAPER • **OPEN ACCESS**

Development of lumped-parameters models for the thermal evaluation and air quality in aircrafts

To cite this article: G Tognon *et al* 2024 *J. Phys.: Conf. Ser.* **2685** 012039

Development of lumped-parameters models for the thermal evaluation and air quality in aircrafts

G Tognon[1,*], P Biasibetti[1] and A Zarrella[1]

[1] Department of Industrial Engineering – Applied Physics Section, University of Padova, Via Venezia 1 – 35131, Padova, Italy

* Corresponding author: giacomo.tognon.2@studenti.unipd.it

Abstract. Aircraft cabins are a challenging category when dealing with thermal comfort and air quality inside means of transport. Two simplified dynamic models are developed. The first one is a lumped resistance-capacitance model for assessing the cabin thermal behaviour during the cruise phase. The fuselage is discretised into several slices and each one is represented through an RC network consisting of eleven nodes, thirteen resistances and three capacities. A thermal balance equation is set for each node and the linear system is solved to calculate the air and surfaces' temperatures. The model is validated by comparison with literature experimental data from ten flights, showing that the predicted temperatures agree well with the measured ones, presenting an RMSE of 1.5, 1.9 and 1.3 °C for cabin air, floor and cabin internal surface temperatures, respectively. A sensitivity analysis is conducted, for which the internal air temperature increases linearly with occupancy rate and decreases with cruising altitude. Secondly, an air quality model is proposed to evaluate the presence of pollutants inside the cabin, based on a simple concentration balance equation. Ventilation flow rates recommended from standards and a recirculation rate below 50-60% should be set to maintain acceptable CO_2 levels.

Keywords: *Lumped resistance-capacitance models, Aircrafts, Indoor Air Quality, Simplified dynamic models.*

1. Introduction

People spend most of their time in indoor spaces enhancing the necessity of providing adequate levels of thermal comfort to safeguard the occupants' well-being. Moreover, the outbreak of COVID-19 pandemic has raised a growing interest in air quality issues. By now, there is strong evidence that the airborne transmission of coronavirus is possible, through virus-laden microdroplets that remain suspended in the air and travel long distances transported by indoor airflows. For this reason, the importance of indoor ventilation for the infection risk mitigation has been increasingly highlighted [1].

Buildings and transport sectors were responsible for about the 40% and 30% of overall energy consumptions in Europe in 2018, leading to relevant GHG emissions [2]. Research is often oriented towards buildings, where the energy use is mainly aimed at maintaining good indoor environmental quality. However, people also use transport to move from one place to another daily. Energy use is primarily related to the vehicle motion, but a significant share is also required to guarantee a comfortable journey for passengers. From this point of view, the aircrafts represent a challenging category. Indeed, flights typically occur at an altitude between 9000 and 12000 m in the troposphere, where the external temperature, pressure and air composition are much different from those at sea level [3]. Additionally, aircrafts are characterized by high occupancy density over a contained volume, which means relevant heat gains and potential increase of CO_2 and other pollutants concentration. The cabin environment has a significant influence on passengers' well-being and health outcomes [4]. Mboreha et al. investigated the relation between COVID-19 spread and ventilation system in aircraft cabin, proposing control strategies regarding the seat arrangement [5]. The air-conditioning system must be well designed; ASHRAE gives guidelines for the environmental control system (ECS) in relation to the fluid dynamics and heat transfer phenomena occurring at high altitude [6].

Thermal comfort and indoor air quality levels achieved inside the passenger cabin can be evaluated experimentally or numerically. Environmental parameters were measured by Cui et al. on ten aircrafts in China; they concluded that thermal environment presents differences between middle, front and

back of the cabin [7]. Mboreha et al. studied numerically temperature and airflow fields in a cabin equipped with distributed inlets above the seat rows for ventilation and compared it to conventional mixing system, showing that the former provides more uniformity and less re-circulation zones, where air quality could worsen [8]. Adopting the same approach, another paper investigates the performance of six innovative personalised ventilation systems in terms of thermal comfort [9]. Konstantinov et al. showed the importance of modelling in a proper way the clothing layer covering passengers' bodies for a realistic prediction of the radiative heat transfer [10]. Allen et al. studied the performance of 30 pilots on 21 manoeuvres in a flight simulator when exposed to different CO_2 concentration, revealing that the odds of passing increase by a factor of 1.69 going from 2500 to 700 ppm [11]. Cao et al. monitored CO_2 concentration in 179 U.S. domestic flights to verify that adequate outside airflow rates were supplied, detecting that only 73% met the recommended minimum of 4.7 l/s per person [12].

Most numerical simulation are based on CFD analysis, resulting computationally expensive. To overcome this issue, simplified modelling techniques are needed. In the case of buildings, several simplified dynamic modelling methods have been conceived, such as lumped parameters models: the building behaviour in terms of heat transfer and accumulation, occurring at the structural elements, is simulated through a resistance-capacitance (RC) network [13]. On the other hand, contaminant dispersion can be suitably evaluated employing a zonal modelling method, setting a simple mass balance within each control volume.

In this paper, two simplified dynamic models are developed. The first one is an RC model of the aircraft for the prediction of air and surface temperatures inside the passenger cabin. Its effectiveness is verified by comparison with data obtained from other literature works. The second one is constructed to assess the trend of pollutants concentration inside the cabin (e.g., CO_2) and the effect of ventilation in keeping acceptable air quality. A sensitivity analysis is carried out with both models to simulate the aircraft cabin behaviour varying different parameters, e.g., occupancy percentage.

2. Methodology

In this section the development and mathematical framework of two simplified models for the simulation of aircraft cabin environment are presented.

2.1. RC model of the cabin

The aircraft cabin is modelled as a resistance-capacitance network, exploiting the thermal-electrical analogy for heat transfer processes. Aircraft thermal characteristics are lumped into parameters that could describe its dynamic behaviour. The thermal resistances represent the branches of the circuit crossed by heat fluxes, whereas the thermal capacities are inserted to include the thermal inertia of massive structures and air volume. The model is thought to be employed for aircrafts of different sizes, from short to long-range flights. In the simulations, only the cruise phase of the flight is considered. From a geometrical point of view, the fuselage is modelled as a cylinder with a constant circular cross section, in relation to the airplane size. It is assumed that cabin rows consist of the same number of seats and are uniformly distributed along the aircraft, without distinguishing between different classes' arrangements. The occupancy density is considered as uniform, excluding the possibility of having cabin areas more crowded than the others. The fuselage internal volume is divided into two distinct spaces by the floor: the passenger cabin (upper part) and the hold (lower part or belly).

Once geometrically defined, the cabin is divided into several slices through parallel cross-sectional planes and the RC network is constructed for each one. The transparent surfaces are considered as evenly distributed along the airplane, dividing the total window area by the number of slices. The network consists of 11 nodes (node temperature denoted with θ), 13 resistances (R) and 3 capacitances (C), as shown in figure 1. Thermal resistances are conductive, convective or radiative based on the type of heat flux they model. Figure 1(a) reports the radiative thermal links between the nodes of the internal surfaces, whereas the convective branches connected to cabin air node are depicted in figure 1(b). The thermal capacities simulate the thermal inertia of fuselage and internal air volume. The former is differentiated between the thermal mass of the upper envelope portion surrounding the

passenger compartment, and the lower part containing the hold, both concentrated at the external nodes. The node state represents the average temperature at specific fuselage surfaces or air volumes. Among the temperature at nodes, θ_{inf} and θ_s are known since they represent the undisturbed external air temperature and the set supply air temperature from the air-conditioning system, respectively. θ_{ext} corresponds to the temperature near the fuselage external surface, and it is directly calculated from θ_{inf} through equation (1), which expresses the rise of air temperature caused by an isentropic compression due to airplane motion at high velocities. In this sense, the parameter R_p is only a fictitious resistance.

$$\theta_{ext} = \left(1 + \frac{\gamma - 1}{2} M^2\right) \theta_{inf} = R_p \theta_{inf} \tag{1}$$

In the equation, γ is the specific heats ratio of air (equal to 1.4) and M is the Mach number determined by the ratio between the aircraft speed (true air speed, TAS) and sound velocity in an ideal gas.

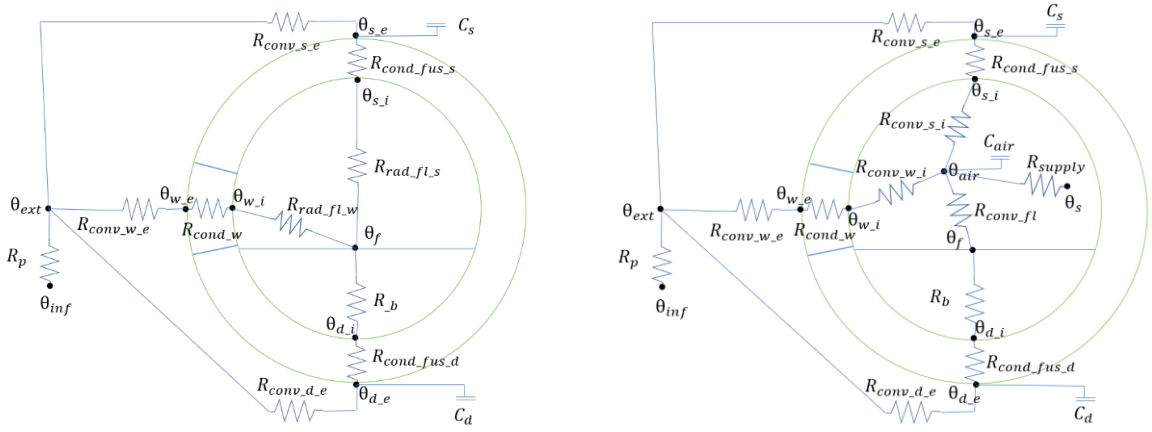

Figure 1. RC network for a fuselage slice, with internal radiative (a) and convective (b) heat exchanges.

The energy balance equations are set for the other eight nodes and the corresponding temperatures θ are determined by solving the resulting linear system at each simulation time step (equation (2) to (9)).

Floor node θ_f

$$\frac{\theta_{d,i} - \theta_f}{R_b} + \frac{\theta_{w,i} - \theta_f}{R_{rad,f,w}} + \frac{\theta_{air} - \theta_f}{R_{conv,f}} + \frac{\theta_{s,i} - \theta_f}{R_{rad,f,s}} + \varphi_{sol,f} + \sum_j (1 - f_{conv,j}) \eta_f \varphi_j = 0 \tag{2}$$

Window internal node $\theta_{w,i}$

$$\frac{\theta_{w,e} - \theta_{w,i}}{R_{cond,w}} + \frac{\theta_{f,i} - \theta_{w,i}}{R_{rad,f,w}} + \frac{\theta_{air} - \theta_{w,i}}{R_{conv,w,i}} = 0 \tag{3}$$

Window external node $\theta_{w,e}$

$$\frac{\theta_{ext} - \theta_{w,e}}{R_{conv,w,e}} + \frac{\theta_{w,i} - \theta_{w,e}}{R_{cond,w}} = 0 \tag{4}$$

Hold internal node $\theta_{d,i}$

$$\frac{\theta_f - \theta_{d,i}}{R_b} + \frac{\theta_{d,e} - \theta_{d,i}}{R_{cond,fus,d}} = 0 \tag{5}$$

Hold external node $\theta_{d,e}$

$$\frac{\theta_{ext} - \theta_{d,e}}{R_{conv,d,e}} + \frac{\theta_{d,i} - \theta_{d,e}}{R_{cond,fus,d}} - \frac{C_d}{\Delta\tau} \left({\theta_{d,e}}^{\tau} - {\theta_{d,e}}^{\tau - \Delta\tau}\right) + \varphi_{sol,fus,d} = 0 \tag{6}$$

Ceiling internal node $\theta_{s,i}$

$$\frac{\theta_{air} - \theta_{s,i}}{R_{conv,s,i}} + \frac{\theta_{s,e} - \theta_{s,i}}{R_{cond,fus,s}} + \frac{\theta_f - \theta_{s,i}}{R_{rad,f,s}} + \varphi_{sol,s,i} + \sum_j (1 - f_{conv,j}) \eta_s \varphi_j = 0 \tag{7}$$

Ceiling external node $\theta_{s,e}$

$$\frac{\theta_{ext} - \theta_{s,e}}{R_{conv,s,e}} + \frac{\theta_{s,i} - \theta_{s,e}}{R_{cond,fus,s}} - \frac{C_s}{\Delta\tau} \left({\theta_{s,e}}^{\tau} - {\theta_{s,e}}^{\tau - \Delta\tau}\right) + \varphi_{sol,fus,s} = 0 \tag{8}$$

Cabin air node θ_{air}

$$\frac{\theta_{w,i} - \theta_{air}}{R_{conv,w,i}} + \frac{\theta_{s,i} - \theta_{air}}{R_{conv,s,i}} + \frac{\theta_f - \theta_{air}}{R_{conv,f}} + \frac{\theta_s - \theta_{air}}{R_{supply}} - \frac{C_{air}}{\Delta\tau} \left({\theta_{air}}^{\tau} - {\theta_{air}}^{\tau - \Delta\tau}\right) + \sum_j f_{conv,j} \varphi_j = 0 \tag{9}$$

In the above equations, θ are the node temperatures [K], R the thermal resistances [K W^{-1}], C the thermal capacitances [J/K], φ_j are the internal heat gains [W], φ_{sol} is the solar radiation load [W], f_{conv} represents the convective fraction of the internal heat gains, and $\Delta\tau$ is the time step length [s]. Infrared and solar radiation are uniformly distributed inside the cabin in proportion to surface area of the node element out of the total (expressed by floor and ceiling area ratio, η_f and η_s). The entering solar radiation share depends on the solar heat gain coefficient (SHGC) of the windows.
The kernel part of the model is the assessment of the lumped parameters. The thermal capacitance of both air and fuselage are obtained through equation (10).

$$C = \rho c_p V \tag{10}$$

where ρ is material density [kg m^{-3}], c_p is the specific heat [J kg^{-1} K^{-1}] and V is the volume of the element. The cabin air density must not be inferior to that of external air at 2440 m above sea level, in compliance with [14]. This minimum value is assumed to calculate air thermal capacity.
The conductive thermal resistances are related to fuselage envelope and window. They can be expressed by equation (11), in a general form for multi-layer structures.

$$R_{cond} = \frac{1}{A_i}\left(\sum_j \frac{s_j}{\lambda_j} + \sum_k r_{cavity,k}\right) \tag{11}$$

Where A_i is the surface area of the element [m^2] s and λ are the thickness [m] and thermal conductivity [W m^{-1} K^{-1}] of each solid layer, and r_{cavity} is the thermal resistance of intermediate cavities [m^2 K W^{-1}]. Convective thermal resistances are calculated through equation (12).

$$R_{conv} = \frac{1}{h_i A_i} \tag{12}$$

where h_i is the convective heat transfer coefficient [W m^{-2} K^{-1}], that has to be estimated based on flow regime and geometry. During the cruise phase, fuselage is affected by forced convection and the coefficient can be determined through equation (13).

$$h_{conv,ext} = \frac{0.74 Re^{-0.2} \rho c_p v}{3.52\ Pr^{0.4}} \tag{13}$$

where Re is Reynolds number, Pr is Prandtl number and v is the aircraft speed [m s^{-1}]. The radiative thermal resistances connecting two surface nodes are determined through equation (14), applying a linearization of the radiative heat exchange.

$$R_{rad,i,j} = \frac{1}{4\sigma A_i F_{ij} {\theta_m}^3} \tag{14}$$

where σ is Stefan–Boltzmann constant equal to 5.67 x 10^{-8} W m^{-2} K^{-4}, F_{ij} is the view factor between i-th and j-th surface, θ_m is the average of the two surfaces temperatures [K]. During the dynamic simulations, in the current calculation time step, T_m is obtained considering the surfaces temperatures of the previous one. The parameter R_b is calculated referring to ISO 6946 [15], considering the hold as a large cavity. Finally, the ventilation-related thermal resistance (R_{supply}) is defined in equation (15).

$$R_{supply} = \frac{1}{\dot{m}_s c_{p,air}} \tag{15}$$

where $\dot{m}_s$ is the supply mass airflow rate [kg s^{-1}], and $c_{p,air}$ is the specific heat of air (1004 J kg^{-1} K^{-1}). The internal heat gains are related to lights, avionics and passengers, who sit down at resting conditions. As reported in equations (2)-(9), they contribute to the heat balance of both air and internal surface nodes, in relation to the convective (f_{conv}) and radiative fraction (1-f_{conv}) of the emitted energy. For the interaction between fuselage and surrounding atmosphere, the radiative exchange with sky is neglected since the forced convective contribution induced by cruise speed is predominant. The undisturbed external air temperature is determined employing the "International Standard Atmosphere" model [3]: it decreases linearly from the sea level (S.L.) up to 11000 m (bottom of tropopause layer), then it is constant until 20000 m (lower boundary of stratosphere), as expressed by equation (16). It is assumed that it remains steady at a given altitude.

$$\theta_{inf}(h) = \begin{cases} \theta_0 + grad\ h & \text{if S.L.} < h < 11000\ \text{m} \\ \theta_{inf}(11000\ \text{m}) & \text{if } h \geq 11000\ \text{m} \end{cases} \quad (16)$$

where h is the aircraft altitude in the cruise phase [m], θ_0 is the reference temperature at sea level and 45° latitude, equal to 288.15 K, and *grad* is a descent gradient of -0.0065 K m^{-1}. The absorbed solar radiation by the *i*-th fuselage portion is calculated through equation (17), assuming that solar radiation impacts on the whole external surface, neglecting the relative orientation between aircraft and sun.

$$\varphi_{sol,fus,i} = A_{fus,i}\ \alpha\ C_y\ I \quad (17)$$

where α is the absorbance of the aluminum, I is the irradiance on a surface at sea level accounting for latitude and hour of day [W m^{-2}], and C_y is a correction factor for solar radiation based on altitude, which accounts for the attenuation effect of the air mass layer crossed by solar rays.
Theoretically, one slice interacts with the adjacent ones, but they are considered as independent, without resistances linking the respective nodes.

2.2. Air quality model

Air quality in the cabin is evaluated through a simplified dynamic model. The cylindrical fuselage is subdivided into slices where a pollutant mass balance is set (e.g., CO_2). It is assumed that each slice has its own inlet and outlet vents for ventilation and does not exchange airflows with the adjacent ones. The contaminant concentration balance, shown in equation (18), is solved at each simulation time step, after the aircraft took off.

$$V\frac{D^{\tau} - D^{\tau-\Delta\tau}}{\Delta\tau} = S + Q_{supply}{D_{supply}}^{\tau} - Q_{out}D^{\tau} \quad (18)$$

Where V is the slice volume [m^3], D is the contaminant concentration in the cabin [ppm], Q_{supply} is the supply flow rate [m^3 h^{-1}], Q_{out} is the exhaust flow rate [m^3 h^{-1}], equal to Q_{supply}, D_{supply} is the contaminant concentration in the fresh air [ppm], S is the contaminant emission rate from occupants [m^3 h^{-1}]. The last parameter depends on person's age and activity level [16], that can be assumed sedentary in the case of an aircraft cabin. The air-conditioning systems in the aircraft typically operate recirculating part of the exhaust air, which mixes with the air from the outside, as outlined in figure 2.

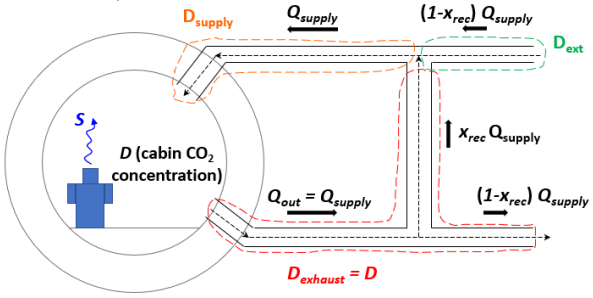

Figure 2. Schematic representation of the air quality model applied to a control volume.

Therefore, the inlet pollutant concentration is determined accordingly through equation (19).

$$D_{supply} = x_{rec}D + (1 - x_{rec})D_{ext} \quad (19)$$

where D and D_{ext} are the cabin exhaust and external pollutant concentrations [ppm], respectively, and x_{rec} is the fraction of recirculated air, ranging from 0 to 1.

3. Applications and results

3.1. RC model validation

The RC model accuracy has been verified comparing its predictions with experimental data from [7]. The tests are conducted on ten flights on a Boeing 737-800, measuring air temperature and surface temperatures on floor, ceiling and side wall; the results are differentiated between front, middle and back part of the aircraft, so the mean values over the entire cabin length are calculated. Ceiling and side wall are represented by a single node in the RC model, thus the average temperature between the two measured values is employed. The obtained results for cabin air node are shown in figure 3.

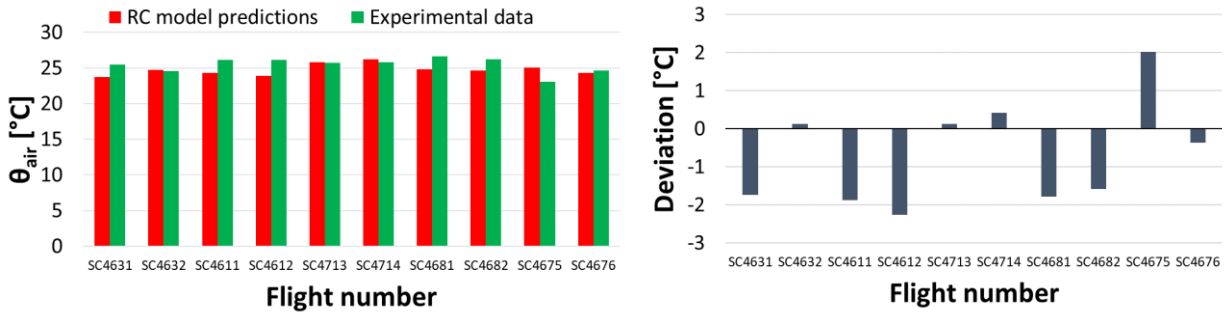

(a) (b)

Figure 3. Comparison (a) and deviations (b) between simulated and measured air temperatures.

From the deviations reported in figure 3(b), the RMSE is calculated through equation (20).

$$RMSE = \sqrt{\frac{\sum_{i=1}^{n}\left(\theta_{sim,i} - \theta_{meas,i}\right)^2}{n}} \tag{20}$$

where θ_{sim} and θ_{meas} are the simulated and measured temperatures [K], respectively, and n is the number of data. The obtained values for the RMSE related to air temperature, floor and cabin internal surface temperatures are 1.5, 1.9 and 1.3 °C, respectively. The larger deviation is observed for the floor node; however, the RC model is sufficiently accurate, and the errors present acceptable values.

3.2. RC model sensitivity analysis

After validation, a sensitivity analysis is conducted employing the RC model to evaluate the thermal behaviour of the cabin varying some parameters. Firstly, the influence of cruising altitude is studied for a Boeing 737-800 at full occupancy and with air conditioning system supplying 9,4 l/s per person at 23°C; the results are shown in figure 4(a) for the cabin air temperature. Three flight heights are chosen, namely 12947 (typical value), 9497 and 7497 m. The temperature decreases with height, but the trend is not linear due to a double aspect: the external temperature decreases linearly only up to 11000 m, then it remains constant, and the air mass layer becomes thinner, leading to lesser weakening of the solar radiation.

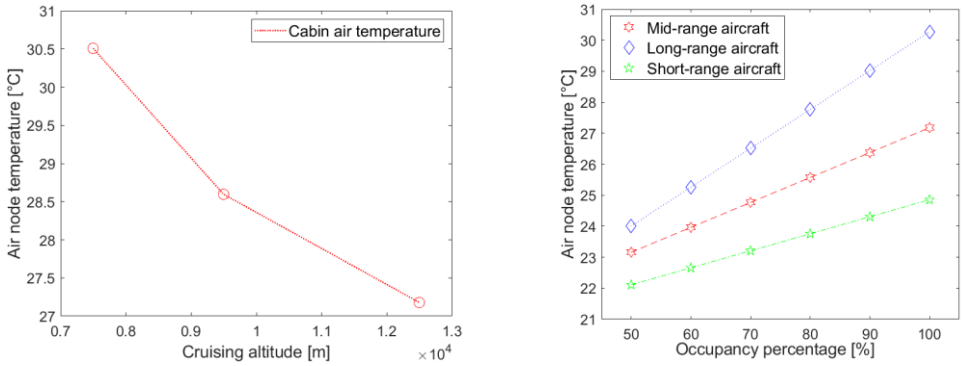

(a) (b)

Figure 4. Sensitivity analysis RC model: effect of cruising altitude (a) and occupancy percentage (b).

In the second instance, the influence of the occupancy percentage on the cabin air temperature, is investigated for a short, a mid and a long-range aircraft, all with similar cruising altitudes. It can be observed from figure 4(b) that the temperature increases linearly with occupancy rate; the long-range aircraft has higher internal air temperatures, whose progressive increase with cabin filling up is larger compared to the other two, as indicated by the slope of the straight lines.

3.3. Air quality model sensitivity analysis

The model for the air quality is employed to assess the CO_2 concentration trend in the cabin under different scenarios during the cruise phase, considering an external CO_2 concentration of 385 ppm and an initial internal of 400 ppm. The average generation rate of one passenger is 0.0032 l/s. In figure 5(a) the effect of occupancy varying between 50 and 100% is highlighted for a Boeing 737-800, where the ventilation flow rate is set at 9.4 l/s per person with 50% of recirculation, according to standards [14], [17]. As expected, the CO_2 concentration at equilibrium is higher for more crowded cabin, and steady state is reached later. In figure 5(b), the trend of steady-state CO_2 concentration as a function of occupancy percentage is reported. A positive linear correlation is observed.

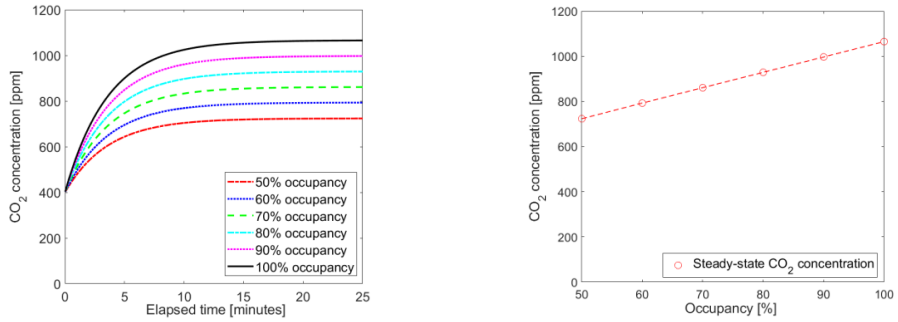

(a) (b)

Figure 5. Effect of occupancy percentage CO_2 concentration trends (a) and steady-state values (b).

The importance of ventilation rate and the effect of recirculation share are also investigated at 100% occupancy for the same aircraft. In the first case, the supply flow rate is varied between 1.4 and 11.4 l/s per passenger, with 50% of recirculation. From the CO_2 trends shown in figure 6(a), it is clear that higher dilution of contaminants is obtained increasing the ventilation flow rate. The time required to reach steady state increases as well; in the worst case it is not reached even after 1 h of flight. In figure 6(b) the effect of recirculation is illustrated, considering a standard supply flow rate of 9.4 l/s per passenger. Energy consumptions for air conditioning can be reduced increasing the recirculation rate, anyway, it should not exceed 50-60% to preserve the air quality in the cabin. At 100% recirculation, the CO_2 concentration increases linearly because the generation is not offset by removal.

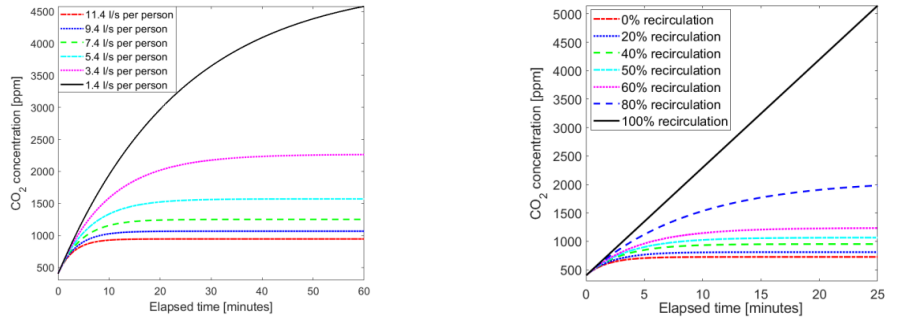

(a) (b)

Figure 6. Effect of ventilation flow rate (a) and percentage of recirculated air (b) on CO_2 balance.

4. Conclusions

In this paper, two simplified dynamic model has been developed to investigate the behaviour of an aircraft cabin, namely a lumped resistance-capacitance (RC) model to simulate the thermal balance of the cabin during the cruise flight, and another for the evaluation of the air quality in the cabin, based on a simple concentration balance for a given contaminant, e.g., CO_2. The validation of the RC model is firstly carried out, then the two models are applied to basic sensitivity analyses to study the influence of different parameters on the cabin environment. These outcomes emerged from the study:

- The comparison with experimental data from literature on a Boeing 737-800 shows good agreement with measurements; RMSEs of 1.5, 1.9 and 1.3 °C are obtained for the cabin air, the floor and the cabin internal surface temperatures, respectively.
- The increase of cruising altitude leads to a non-linear decrease in the cabin air temperature due to the double effect of external temperature drop and reduction of the air mass layer attenuating the solar radiation; instead, air temperature increases linearly with occupancy rate.
- The CO_2 steady concentration increases linearly and is reached later with higher occupancy percentages; the ventilation flow rate should be compliant with values recommended by the standards and the recirculation rate should be kept below 50-60% to preserve cabin air quality.

The proposed models present some limitations and need further improvements. At the moment, the passengers are supposed to uniformly distribute inside the cabin. Moreover, the slices into which the fuselage is discretised are considered as independent, whereas it would be interesting to include link branches between air nodes of adjacent cells, enabling the air movement across different sub-volumes.

5. References

[1] L. Morawska *et al.*, "How can airborne transmission of COVID-19 indoors be minimised?," *Environment International*, vol. 142. Elsevier Ltd, Sep. 01, 2020.
[2] European Commission. Statistical Office of the European Union (Eurostat), *Energy data 2020 edition*. 2020.
[3] NOAA, NASA, and USAF, *U.S. Standard Atmosphere*. Washington, D.C.: U.S. Government Printing Office, 1976, 1976.
[4] H. Hinninghofen and P. Enck, "Passenger well-being in airplanes," *Auton Neurosci*, vol. 129, no. 1–2, pp. 80–85, Oct. 2006.
[5] C. A. Mboreha and G. Kumar, "RISK AND PREVENTING OF COVID-19 IN A COMMERCIAL AIRCRAFT CABIN: AN OVERVIEW," *International Journal of Engineering Applied Sciences and Technology*, vol. 5, 2020.
[6] ASHRAE, "ASHRAE Handbook 2019 - HVAC Applications," 2019.
[7] W. Cui, Q. Ouyang, and Y. Zhu, "Field study of thermal environment spatial distribution and passenger local thermal comfort in aircraft cabin," *Build Environ*, vol. 80, pp. 213–220, 2014.
[8] C. A. Mboreha *et al.*, "Numerical simulations of the flow fields and temperature distribution in a section of a Boeing 767-300 aircraft cabin," *Mater Today Proc*, vol. 47, pp. 4098–4106, 2021.
[9] C. A. Mboreha *et al.*, "Investigation of thermal comfort on innovative personalized ventilation systems for aircraft cabins: A numerical study with computational fluid dynamics," *Thermal Science and Engineering Progress*, vol. 26, Dec. 2021.
[10] M. Konstantinov *et al.*, "Numerical simulation of the air flow and thermal comfort in aircraft cabins," *Notes on Numerical Fluid Mechanics and Multidisciplinary Design*, vol. 124, pp. 293–301, 2014.
[11] J. G. Allen *et al.*, "Airplane pilot flight performance on 21 manoeuvres in a flight simulator under varying carbon dioxide concentrations," *J Expo Sci Environ Epidemiol*, vol. 29, no. 4, pp. 457–468, Jun. 2019.
[12] X. Cao *et al.*, "The on-board carbon dioxide concentrations and ventilation performance in passenger cabins of US domestic flights," *Indoor and Built Environment*, vol. 28, no. 6, pp. 761–771, Jul. 2019.
[13] European Committee for Standardization-CEN, *EN ISO 13790:2008, Energy performance of buildings-Calculation of energy use for space heating and cooling*. 2008.
[14] Federal Aviation Administration (FAA), *FAR 14 CFR 25.831. Part 25-Airworthiness standards: transport category airplanes.* Washington, DC, 2013.
[15] European Committee for Standardization-CEN, *EN ISO 6946:2017, Building components and building elements - Thermal resistance and thermal transmittance - Calculation methods*. 2017.
[16] A. Persily and L. de Jonge, "Carbon dioxide generation rates for building occupants," *Indoor Air*, vol. 27, no. 5, pp. 868–879, Sep. 2017.
[17] ANSI/ASHRAE, *Standard 161-2007 Air quality within commercial aircrafts*. Atlanta, GA, 2007.